Nano Research 2014, 7(4): 443–452
DOI 10.1007/s12274-014-0410-6
Research Article
ISSN 1998-0124
CN 11-5974/O4

Flexible thermocells for utilization of body heat

Hyeongwook Im[1], Hyung Geun Moon[2], Jeong Seok Lee[1], In Young Chung[2], Tae June Kang[3] (✉), and Yong Hyup Kim[1] (✉)

[1] *School of Mechanical and Aerospace Engineering, Seoul National University, Seoul 151-742, Republic of Korea*
[2] *Department of Electronics and Communications Engineering, Kwangwook University, Seoul 139-701, Republic of Korea*
[3] *Department of Nanofusion Technology, Pusan National University, Busan 609-735, Republic of Korea*

Received: 12 October 2013
Revised: 21 December 2013
Accepted: 8 January 2014

KEYWORDS

wearable thermocell,
body heat,
waste heat recovery,
carbon nanotubes,
activated carbon textile,
porous electrode

ABSTRACT

Plastic thermo-electrochemical cells (thermocells) involving aqueous potassium ferricyanide/ferrocyanide electrolyte have been investigated as an alternative to conventional thermoelectrics for thermal energy harvesting. Plastic thermocells that consist of all pliable materials such as polyethylene terephthalate (PET), fabrics, and wires are flexible enough to be wearable on the human body and to be wrapped around cylindrical shapes. The performance of the thermocells is enhanced by incorporating carbon nanotubes into activated carbon textiles, due to improved charge transfer at the interface. In cold weather conditions (a surrounding temperature of 5 ˚C), the thermocell generates a short-circuit current density of 0.39 A/m^2 and maximum power density of 0.46 mW/m^2 from body heat (temperature of 36 ˚C). For practical use, we have shown that the thermocell charges up a capacitor when worn on a T-shirt by a person. We also have demonstrated that the electrical energy generated from waste pipe heat using a serial array of the thermocells and voltage converters can power a typical commercial light emitting diode (LED).

The human body consistently maintains its temperature at 36 ˚C for its whole life and simultaneously releases thermal energy of about 100 watts to the surroundings [1]. Based on Carnot efficiency, a maximum power of about 5 watts [2]—which is equivalent to the power needed to operate a portable smart electronic device—is available from the released body heat [3]. Recently, low power technology has become more feasible, due to the progressive advances in electronic devices, so that the energy scavenged from body heat is expected to either replace or augment battery usage [4, 5].

Thermoelectric generators are envisioned as a host for harvesting low-grade thermal energy. In the past decades, numerous advances have been made in thermoelectric devices [4, 6–10], the basic unit of which typically consists of n-type and p-type semiconductors. However, the relatively small thermoelectric coefficient (~tens of microvolts per Kelvin) is the main obstacle

Address correspondence to Tae June Kang, tjkang@pusan.ac.kr; Yong Hyup Kim, yongkim@snu.ac.kr

to harvesting of thermal energy, which is typically available at temperatures below 100 ℃ [11]. Moreover, there still remain obstacles such as rare and fragile thermoelectric materials and complicated fabrication processes being required [12, 13].

In the present study, we report an efficient method that converts low-grade waste thermal energy such as heat released from the human body into electricity using an all-carbon electrode with hierarchical porosity that is designed for a thermal electrochemical cell (thermocell). The thermocell presented here utilizes the temperature dependence of the ferricyanide/ferrocyanide ($Fe(CN)_6^{3-}$/$Fe(CN)_6^{4-}$) redox potential and employs the flexibility of an activated carbon textile (ACT) electrode that is coated with carbon nanotubes (CNTs). With these components, the thermocell is flexible enough to wear on clothes and to wrap around cylindrical shape such as pipes. The wearability for harnessing human body heat is demonstrated by means of a plastic thermocell connected to a capacitor that is embedded into a T-shirt, which is in turn worn by a person. Practical use of the thermocell is demonstrated with a serial thermocell array that can power a typical commercial light emitting diode (LED).

To fabricate a thermocell that is pliable enough to accommodate any shape of heat source including a body or curved shape, we developed a plastic thermocell that consists of all flexible materials such as polyethylene terephthalate (PET), fabrics, and wires (Figs. 1(a) and inset of Fig. 1(b)). The thermocell was fabricated by a one-step process of placing separator and adhesive tape between two half-cells, and then hot pressing them at 120 ℃ for 20 s, the half-cell being PET, collecting wire, and CNT-coated ACT (C-ACT) stacked in order.

The fabricated thermocell is 600 μm thick and has a highly flexible nature. A 0.4 M ferricyanide/ferrocyanide redox couple, the concentration of which is close to saturation, was used as an aqueous electrolyte. The thermoelectric coefficient of the redox couple was obtained by measuring the temperature dependence of the potential difference over a temperature range from

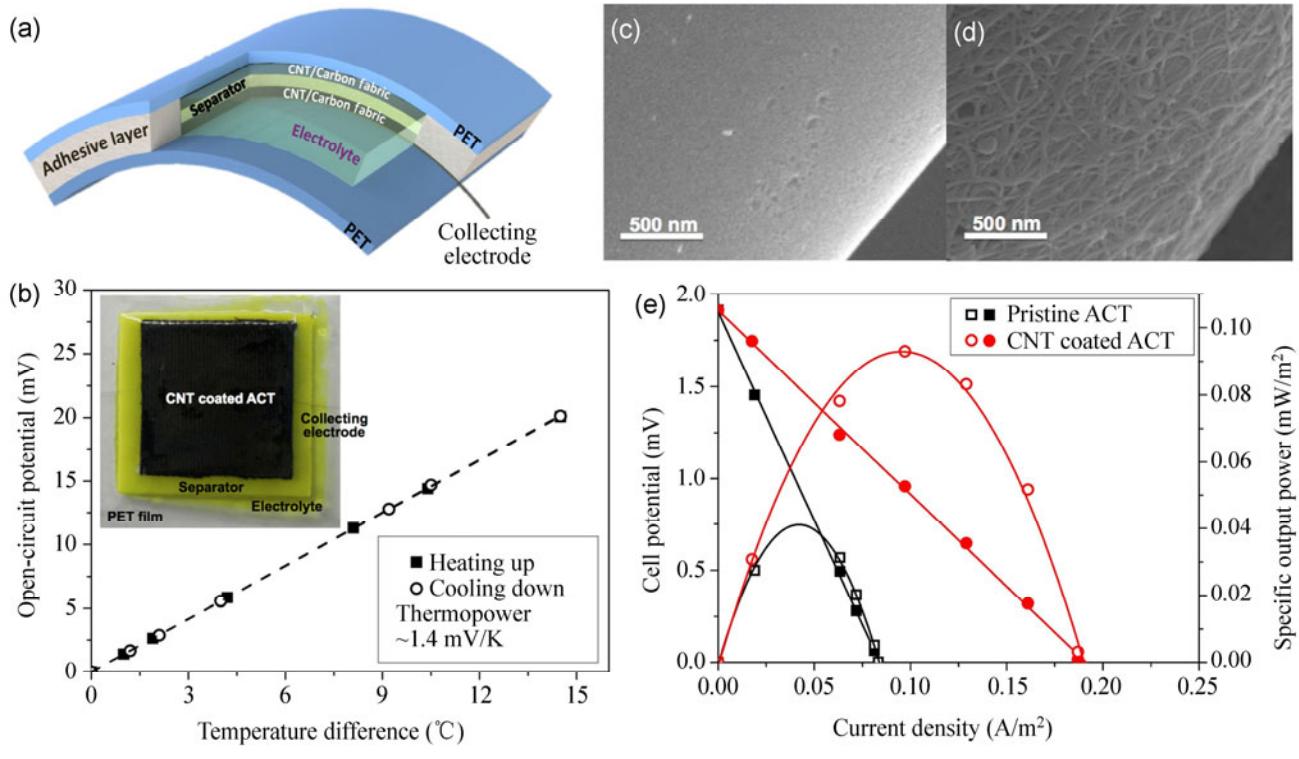

Figure 1 (a) Schematic depicting the structure of the flexible thermocell. (b) Dependence of open-circuit potential on the temperature difference between hot and cold electrodes (Inset: Photograph of the plastic thermocell). SEM images of the (c) pristine and (d) CNT-coated activated carbon textile (ACT). (e) Thermocell discharge and specific output power as a function of the current density of pristine the ACT and C-ACT electrodes.

0 to 15 ℃, as shown in Fig. 1(b). The thermoelectric coefficient (~1.4 mV/K) is in good agreement with previous reports (1.4 to 1.6 mV/K) [14–16]. Compared with other redox couples such as Cu^{2+}/Cu, Fe^{2+}/Fe and Np^{4+}/Np^{3+}, the ferricyanide/ferrocyanide electrolyte is better suited for harvesting low-grade thermal energy by virtue of its relatively higher thermoelectric power and larger exchange current density [17, 18].

For the choice of electrode material, charge transfer reaction and activation barrier at the electrode/electrolyte interface have to be considered because they are the two most important factors that determine the electrochemical performance. The electrode performance is generally related to surface area and catalytic behavior of electrodes [19, 20]. Activated carbon textiles having a high specific surface area are good candidates for electrode materials [21–23]. Moreover, carbon nanotubes have been widely employed in electrochemical applications due to fast carrier transportation, superior chemical stability and excellent catalytic activity [24–26]. Therefore, the performance of the device is expected to be enhanced by incorporating CNTs into the ACT electrode sheet. In addition, the flexible feature of the textile allows fabrication of a pliable thermocell that is compatible with curved heat sources.

Inspired by the solution-based CNT coating method [27], the CNT-coated textile sheet was simply prepared by dipping ACT into a colloidal solution of CNTs, followed by drying in oven (the detailed experimental procedure is given in the experimental section). The fabrication process is similar to that widely used dyeing fibers and fabrics in the textile industry. It was observed that the CNT solution instantly soaked into the textile and the CNT networks formed conformally on the surface of the individual textile fibers, as shown in Figs. 1(c) and 1(d).

We compared the performance of the thermocell with ACT against that with a C-ACT electrode. As shown in Fig. 1(e), the C-ACT electrode yielded a current density (j_{SC}) of 189.25 mA/m^2 and a power density (P_{MAX}) of 90.38 μW/m^2, corresponding to a normalized current density ($j_{SC}/\Delta T$) of 139.15 mA/m^2·K and a normalized specific power density ($P_{MAX}/\Delta T^2$) of 48.86 μW/m^2·K^2, values which are much higher than the corresponding ones for the thermocell with pristine ACT—62.32 mA/m^2·K and 21.9 μW/m^2·K^2, respectively. The enhanced performance of the C-ACT electrode can be explained by the reduction of three primary internal resistances (Fig. 2(a)), i.e., activation, ohmic and mass transport overpotentials.

It is well known that CNTs have fast electron transfer characteristics due to their high local density of states and quasi-reversible redox process [16, 28]. Therefore, coating CNT on an ACT electrode might reduce the activation barrier in thermocell reaction [20]. Cyclic voltammetry (CV) measurements were carried out to compare reaction characteristics of ACT and C-ACT electrodes. It is clearly observed from Fig. 2(b) that the redox potential difference decreased from 239 to 135 mV after introducing CNTs. Furthermore, as shown in Fig. 2(c), the diameter of the semi-circle on the complex plane in the Nyquist plot was smaller for the C-ACT electrode compared to the ACT electrode. Note that the diameter of the semi-circle represents the kinetic resistance (R_{ct}) of the Faradaic reaction based on the Randle's equivalent circuit model [29, 30] shown in the inset of Fig. 2(c). These measurements indicate that the CNT coated on the ACT electrode gives the benefit of lowering the activation barrier in thermocell reactions. Because of the improved reaction characteristics, the activation overpotential was significantly reduced by 63% (from 27.4 to 10 Ω) as shown in Fig. 2(a).

Ohmic overpotential in a thermocell is caused by equivalent series resistance (ESR), typically composed of electrode and electrolyte resistances. While changes in electrical resistance of electrolyte are negligible because both thermocells have same inter-electrode spacing and electrolyte concentration, the CNT coated on ACT leads to almost a fivefold decrease in the sheet resistance of ACT (from 14 to 3 Ω/sq.) as shown in Fig. 2(d). From the analysis of electrochemical impedance spectroscopy (EIS) measurements, it is confirmed that the ESR decreased from 17.5 to 14.6 Ω when the C-ACT is utilized (Fig. 2(c)).

A mass transport process is needed to transfer the reaction product formed at one electrode to the other electrode for continuous operation in a thermocell [31]. In general, diffusion processes due to both thermal (Soret diffusion) and concentration (Fickian diffusion) gradients, and convective process due to density

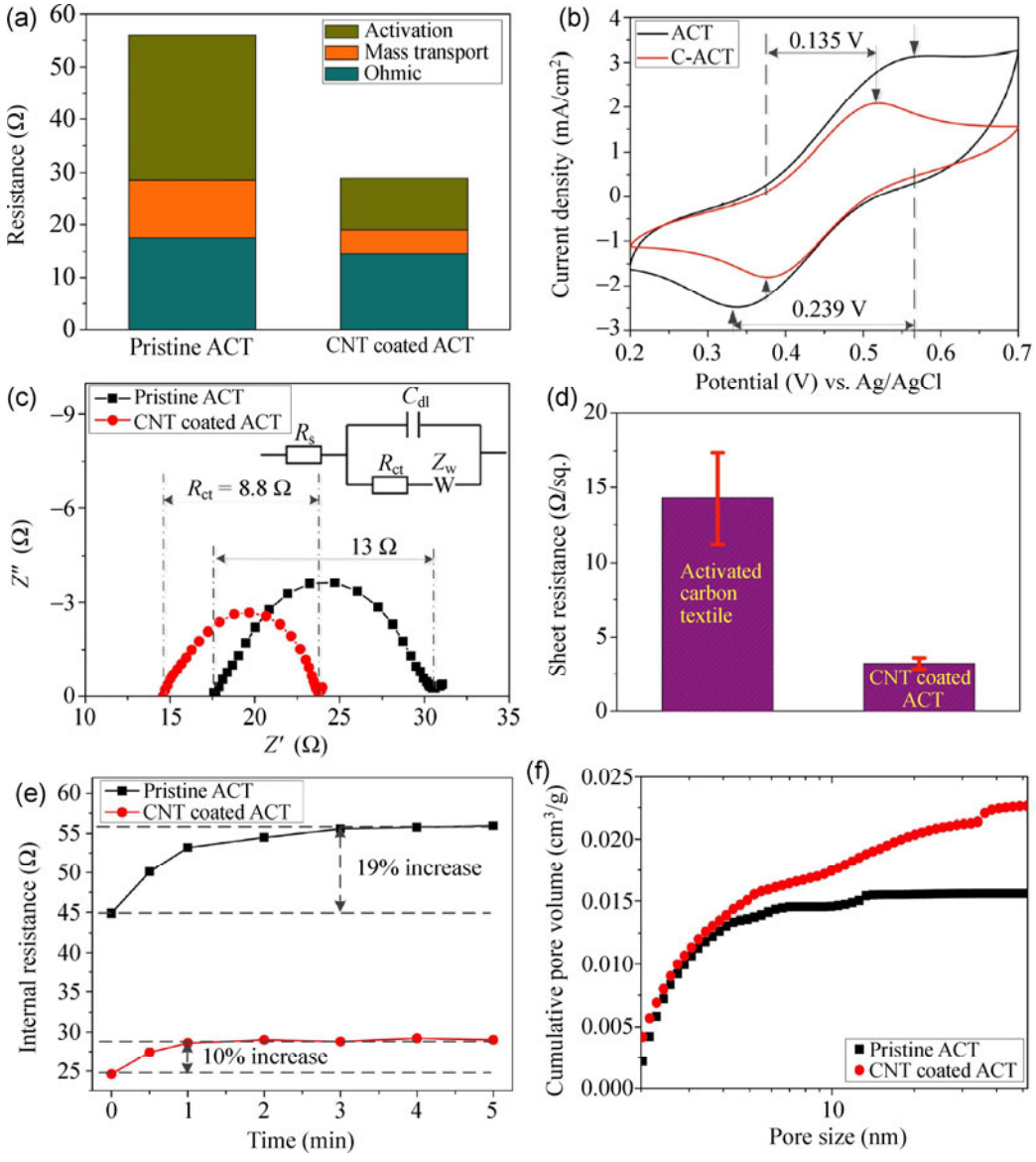

Figure 2 (a) Comparison of three internal overpotentials of the thermocell with pristine ACT and C-ACT electrodes. (b) Cyclic voltammogram of pristine and CNT-coated ACT sheet. (c) Nyquist impedance plots for ACT and C-ACT electrodes. Inset shows the Randle's equivalent circuit. (d) Sheet resistance of the two textile electrodes. (e) Time-dependent overall internal resistance change of the thermocell with ACT and C-ACT electrodes. (f) The cumulative pore volume in the mesopore range derived using non-local density function theory (NLDFT).

gradients [32–35] contribute to mass transport in thermocells. Therefore, mass transport overpotential can be evaluated by measuring the time dependence of internal resistance of the thermocell (Fig. 2(e)). Though a highly porous electrode composed of micropores only, such as ACT, has significant advantages in terms of providing large electrochemical reaction sites, it might hinder the mass transport of reactants and products. We note in this regard that an electrode with hierarchical pore structure facilitates enhanced diffusion of ions into the electrode, as in vascular structures in nature [36–40]. Analyses of the pore size distributions of ACT and C-ACT electrodes were performed using the Brunauer–Emmett–Teller (BET) method. It is noteworthy from Fig. 2(f) that the cumulative pore volume of C-ACT increases with increasing pore size from micropores to mesopores in contrast to the ACT, which shows a cumulative

volume saturated at micropores. The hierarchical feature of C-ACT pores is expected to improve mass transport overpotential by contributing to enhanced ion transport. As shown in Fig. 2(e), the increase in the internal resistance of the thermocell with a C-ACT electrode is relatively smaller than that with ACT and the resistance settles quickly down to a steady state within 60 s.

Discharge characteristics of the thermocell are shown in Fig. 3. The voltage–current (*E*–*I*) relationship is given in Fig. 3(a) as a function of time. In the measurements, the operating temperature—which is defined as the average of the temperatures at the hot and cold electrodes—was fixed at 20.5 ℃ and the temperature difference was maintained at 3.4 ℃. The working area (C-ACT electrode size) was 2 cm × 2 cm. The internal resistance, i.e., the slope of the *E*–*I* curve, increases during cell discharge, reaching a steady state of 30.5 Ω (the inset of Fig. 3(a)). Due to the relatively short traveling path of ions (about 100 μm) and hierarchical porous structure of the electrode, the steady-state discharge of the thermocell could be reached within 1 min. The resistance variation from the initial to the steady state was measured to be 1.7 Ω. The cell potential and specific output power as a function of the current density at steady state is shown in Fig. 3(b). It can be seen that the plastic thermocell generated j_{SC} of 0.39 A/m^2 (current of 152 μA) and P_{MAX} of 0.46 mW/m^2 (output power of 184 nW), indicating that power generation from body heat is feasible.

To explore the feasibility of power generation from a human body, the ambient temperature for the thermocell was varied, ranging from 5 ℃ (cold weather) to 30 ℃ (hot weather), while the other electrode was maintained at 36 ℃, which is the human body temperature. Because of the relatively high thermal resistance of the PET substrate, the temperature drop mainly occurs across the outer substrate layer (see the Electronic Supplementary Material (ESM)), so that an ambient temperature of 5 ℃ with the other electrode maintained at 36 ℃ yielded a temperature difference of 3.4 ℃. In Fig. 4, ambient temperatures of 10, 20, and 30 ℃ correspond to actual temperature differences of 2.9, 1.8, and 0.6 ℃, respectively. As shown in Fig. 4(a), the open-circuit potential (V_{OC}) increases with increasing temperature difference, resulting in a quadratic increase of the maximum power generated, P_{MAX}, which increases from 0.02 mW/m^2 for ΔT = 0.6 ℃ to 0.46 mW/m^2 for ΔT = 3.4 ℃ (Fig. 4(b)). For the maximum temperature difference used in the experiment (i.e., an operating temperature of 20.5 ℃), the thermocell gave a normalized current density of 0.114 A/m^2·K and a normalized maximum power density of 39.56 μW/m^2·K^2.

As shown in Fig. 4(c), the internal resistance decreases with increasing operating temperature. An increase in the temperature should lead to an improvement in ion transport through the separator and also diffusion within the electrodes [31], resulting in an enhancement of the mass transport (Fig. S2 in

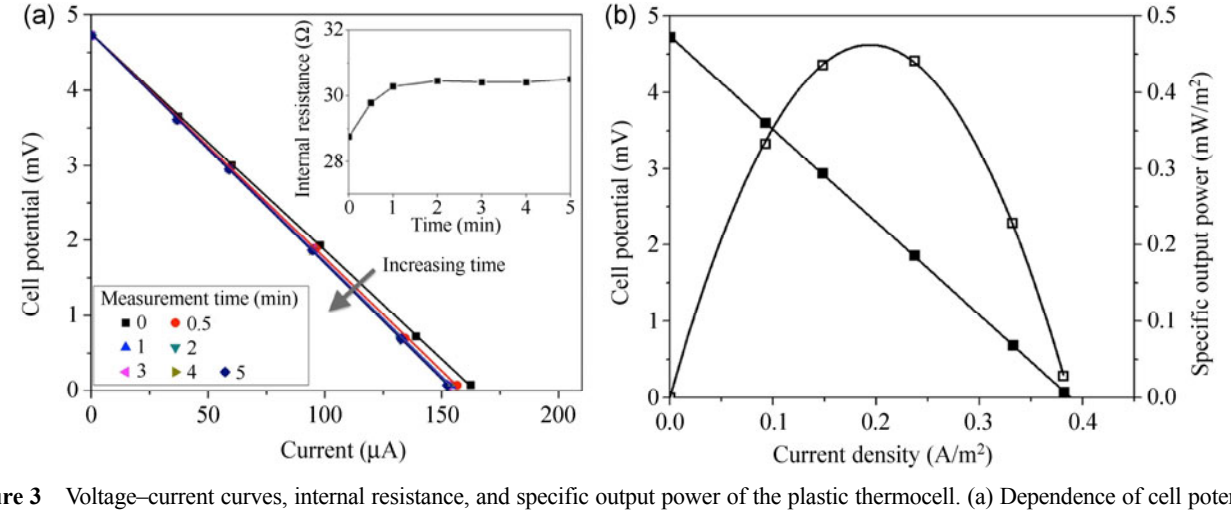

Figure 3 Voltage–current curves, internal resistance, and specific output power of the plastic thermocell. (a) Dependence of cell potential on current with increasing time from the start of energy harvesting. The inset shows the dependence of internal resistance on time. (b) Plots of cell potential (solid squares) and specific output power (open squares) versus current density at steady state.

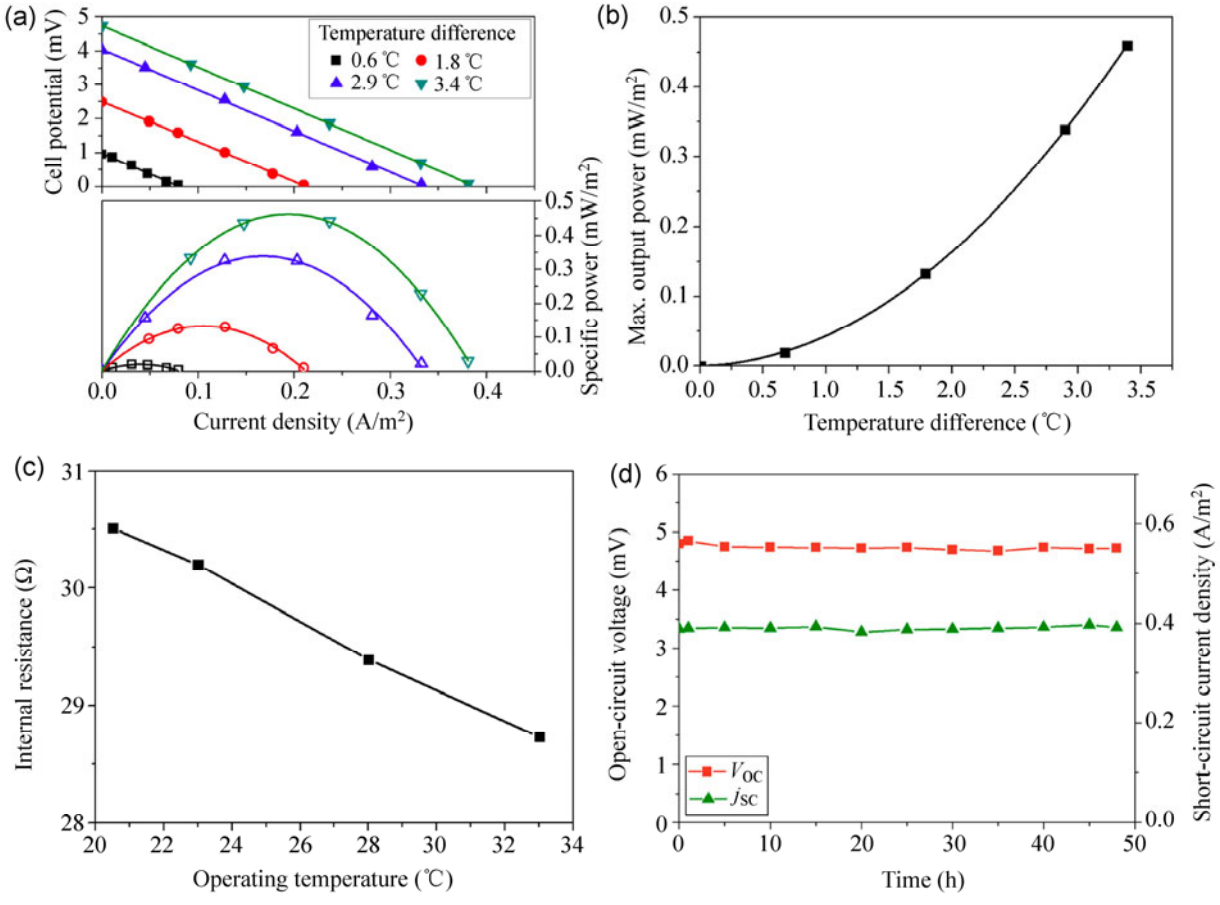

Figure 4 Effect of temperature difference on (a) *E–I* curves and output power versus current density and (b) maximum specific output power. (c) Dependence of internal resistance on operating temperature. (d) Dependence of open-circuit voltage and short-circuit current density on time with a temperature difference of 3.4 ˚C.

the ESM). This enhancement is confirmed by the result that the thermocell provided $j_{SC}/\Delta T$ of 0.122 A/m²·K and $P_{MAX}/\Delta T^2$ of 42.83 μW/m²·K² at the high operating temperature of 33 ˚C, values which are higher than those at an operating temperature of 20.5 ˚C. The thermocell produced stable values of V_{OC} and j_{SC} during 48 h of operation (Fig. 4(d)), which indicates that the device should be stable in long-term operation.

A good way to harness the heat from a human body is to attach the thermocell to a shirt. As a demonstration, a T-shirt embedded with the plastic thermocell was connected to a capacitor which could be charged up by the power generated from the thermocell (inset of Fig. 5(a)). The capacitor has a structure identical to that of the plastic thermocell, the only difference being the electrolyte of 1.0 M KCl solution. Figure 5(a) shows the charge/discharge behavior of the capacitor when the shirt was put on and off, demonstrating that the body heat can be harvested effectively with the thermocell T-shirt (power output of 11.7 nW).

A large source of waste heat can be found in power plants or various industrial facilities where large amounts of waste heat are lost through numerous pipes that carry hot fluids [41]. This waste heat can be harvested when a thermocell is employed. As proof of concept we used a flexible thermocell wrapped around a pipe with various curvatures, as depicted in the inset of Fig. 5(b). The power generated from the thermocell without curvature, P_0, was 0.54 mW/m² with a pipe temperature of 80 ˚C and an ambient temperature of 24 ˚C. It is interesting to observe that the power from the thermocell increases by more than 30% when it is wrapped around pipe (Fig. 5(b)), although the incremental increase diminishes as the curvature is increased. The increase could be attributed

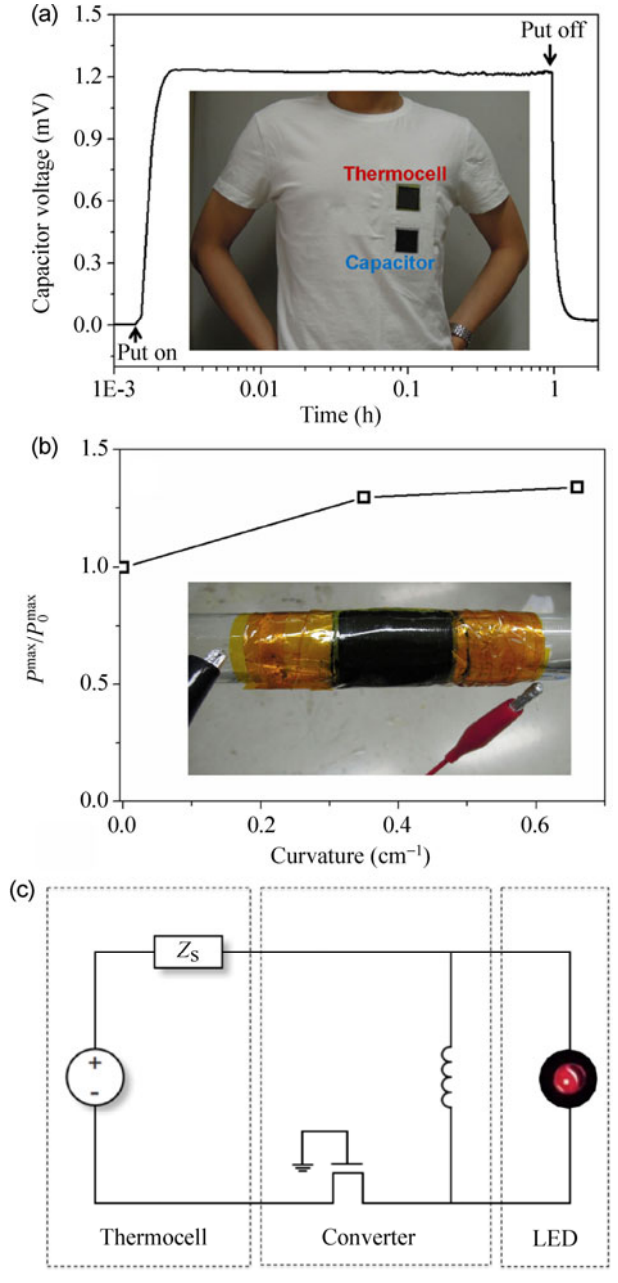

Figure 5 (a) Charge/discharge of a capacitor connected to the thermocell. Inset: Photograph of the T-shirt embedded with the thermocell and capacitor, the latter for storing the power generated from the thermocell. (b) Normalized maximum power output for various curvature radii. Inset: Photograph of a thermocell wrapped around a hot fluid pipe for energy harvesting. (c) Circuit diagram depicting the lighting system for the LED, composed of thermocell, voltage converter and LED (the actual red light of the LED is shown within the dark circle in the LED part).

to the reduced contact resistance between the collecting wire and the textile electrode caused by the compression created when the thermocell is wrapped around the pipe.

A question that should be raised is whether the low power scavenged from low level heat sources can ever be put to good use. Although progressive advances in electronics should enable good use of the low power to the point of either replacing or augmenting battery usage with even human body heat, we show here that a commercial LED can be turned on with the thermocell fabricated here. For this purpose, four-serial plastic thermocells and a home-made voltage converter circuit were used, as shown in Fig. 5(c). The serially connected thermocells generated a voltage of about 100 mV from a pipe with hot water of 80 °C. Since the generated voltage is not high enough to light up a commercial LED with typical turn-on voltage of about 1.5 V, the output voltage was boosted using the converter circuit. The serially connected thermocell, modeled as an ideal source and a series resistance, is connected to an inductor through a transistor, which is used as a switch device and controlled by periodic pulses. With the converter circuit, the LED was turned on and stayed on. The actual red light from the LED is shown within the dark circle in the LED part of Fig. 5(c).

In summary, we have developed a plastic thermocell that is flexible enough to be wearable on the human body and to be wrapped around cylindrical shapes. Hierarchical porous textiles coated with CNTs were also developed as an electrode to enhance the thermocell performance by lowering the three primary overpotentials. We have shown that the thermocell charges up a capacitor when worn by a person on a T-shirt with a maximum output power density of 0.46 mW/m^2. We have demonstrated that the electrical energy generated from waste pipe heat by a serial array of the thermocells can power a typical commercial LED whose turn-on voltage is 1.5 V. The results indicate that the thermocell developed here can serve as a self-sustainable energy source. The flexible thermo-electrochemical device introduced here should inspire further research in the area of waste heat recovery.

Experimental

Material preparation. In order to obtain activated carbon textiles (ACT, CH15, Kuraray Chemical, Japan) coated with CNTs, it is necessary to prepare a

well-dispersed colloidal solution of CNTs. We used commercially available purified single-walled carbon nanotubes (SWNT, ASP-100F produced by Il-jin Nanotech) and dodecylbenzenesulfonate (SDBS, Sigma-Aldrich) as an anionic surfactant to make the SWNT colloidal solution. SWNTs were added to 57 mM SDBS aqueous solution at a concentration of 2 mg/mL followed by dispersal using ultrasonication for 12 h. C-ACT was obtained by simple dipping and drying process. When pristine ACT was dipped into the colloidal solution, the ACT quickly swelled with a large amount of the solution due to its highly porous structure. The C-ACT was subsequently rinsed with deionized water (DIW) several times to remove redundant SDBS, and then dried in an oven.

An aqueous electrolyte of 0.4 M potassium ferricyanide ($K_3Fe(CN)_6$, Sigma Aldrich) and potassium ferrocyanide ($K_4Fe(CN)_6$, Sigma Aldrich) was used for the thermocell, while an aqueous electrolyte of 1.0 M potassium chloride (KCl, Sigma Aldrich) was used for the capacitor.

For the half-cell, PET, collecting wire, and CNT-coated ACT were stacked in order. Then, separator and adhesive tape were placed between two half-cells. The thermocell structure was completed by one-step hot pressing process at 120 ˚C for 20 s.

Characterization. Hot and cold temperatures were controlled by circulating water from a thermostatic bath with an accuracy of ± 0.1 ˚C. The potential and current output from the cell were measured using a voltage–current meter (Keithley, 2000 Multimeter) for characterizing power output with respect to external resistive loads. Sheet resistance of the samples was simply measured by a four-point probe instrument (Changmin Tech, CMT-SR2000N). Electrochemical impedance measurements were conducted using a commercial instrument (Zahner, IM6ex). N_2 adsorption isotherms (at 77 K) up to 1 bar were measured using a Micromeritics ASAP 2020 static volumetric gas adsorption instrument. Prior to the sorption analysis, samples in the analysis chamber were subject to a vacuum of 10^{-5} Torr at 150 ˚C for 12 h to remove the impurities. The cyclic voltammetry (Eco Chemie, PGSTAT30) analysis was carried out using ACT and C-ACT as a working electrode in 10 mM $K_4Fe(CN)_6$ solution with a scan rate of 5 mV/s. Platinum (Pt) and saturated calomel electrodes were used as counter and reference electrodes, respectively.

Acknowledgements

This work was supported by National Research Foundation of Korea grants funded by the Korean government (Grant Nos. 2011-0024818, 2009-0078659, and 2009-0083512), K-water Research and Business Project (No. K_RBP-1), the Pusan National University Research Grant 2012 funded by Pusan National University, the Research Grant of Kwangwoon University in 2012 and a grant from the Civil and Military Technology Cooperation Program through the National Research Foundation of Korea (NRF) funded by the Ministry of Science, ICT and Future Planning (No. 2013M3C1A9055407). The authors also acknowledge support from the Institute of Advanced Aerospace Technology at Seoul National University.

Electronic Supplementary Material: Supplementary material (analysis of thermal resistances of PET and electrolyte, change of mass transport resistance with respect to operating temperature and power conversion efficiency) is available in the online version of this article at http://dx.doi.org/10.1007/s12274-014-0410-6.

References

[1] Qi, Y.; McAlpine, M. C. Nanotechnology-enabled flexible and biocompatible energy harvesting. *Energy Environ. Sci.* **2010**, *3*, 1275–1285.

[2] Hirai, T.; Shindo, K.; Ogata, T. Charge and discharge characteristics of thermochargeable galvanic cells with an $[Fe(CN)_6]^{4-}/[Fe(CN)_6]^{3-}$ redox couple. *J. Electrochem. Soc.* **1996**, *143*, 1305–1313.

[3] Vullers, R. J. M.; van Schaijk, R.; Doms, I.; Van Hoof, C.; Mertens, R. Micropower energy harvesting. *Solid-State Electron.* **2009**, *53*, 684–693.

[4] Leonov, V.; Torfs, T.; Fiorini, P.; Van Hoof, C. Thermoelectric converters of human warmth for self-powered wireless sensor nodes. *IEEE Sens. J.* **2007**, *7*, 650–657.

[5] Aydin, E. A.; Güler, I. Recent advances on body-heat powered medical devices. *Recent Patents on Biomedical Engineering* **2011**, *4*, 33–37.

[6] Snyder, G. J.; Lim, J. R.; Huang, C. K.; Fleurial, J. P. Thermoelectric microdevice fabricated by a MEMS-like electrochemical process. *Nat. Mater.* **2003**, *2*, 528–531.

[7] Weber, J.; Potje-Kamloth, K.; Haase, F.; Detemple, P.; Völklein, F.; Doll, T. Coin-size coiled-up polymer foil thermoelectric power generator for wearable electronics. *Sensor. Actuat. A-Phys.* **2006**, *132*, 325–330.

[8] Kraemer, D.; Poudel, B.; Feng, H. P.; Caylor, J. C.; Yu, B.; Yan, X.; Ma, Y.; Wang, X.; Wang, D.; Muto, A., et al. High-performance flat-panel solar thermoelectric generators with high thermal concentration. *Nat. Mater.* **2011**, *10*, 532–538.

[9] Settaluri, K. T.; Lo, H. Y.; Ram, R. J. Thin thermoelectric generator system for body energy harvesting. *J. Electron. Mater.* **2012**, *41*, 984–988.

[10] Hewitt, C. A.; Kaiser, A. B.; Roth, S.; Craps, M.; Czerw, R.; Carroll, D. L. Multilayered carbon nanotube/polymer composite based thermoelectric fabrics. *Nano Lett.* **2012**, *12*, 1307–1310.

[11] Abraham, T. J.; MacFarlane, D. R.; Pringle, J. M. Seebeck coefficients in ionic liquids-prospects for thermo-electrochemical cells. *Chem. Commun.* **2011**, *47*, 6260–6262.

[12] Snyder, G. J.; Toberer, E. S. Complex thermoelectric materials. *Nat. Mater.* **2008**, *7*, 105–114.

[13] Vining, C. B. An inconvenient truth about thermoelectrics. *Nat. Mater.* **2009**, *8*, 83–85.

[14] Quickenden, T. I.; Vernon, C. F. Thermogalvanic conversion of heat to electricity. *Sol. Energy* **1986**, *36*, 63–72.

[15] Mua, Y.; Quickenden, T. I. Power conversion efficiency, electrode separation, and overpotential in the ferricyanide/ferrocyanide thermogalvanic cell. *J. Electrochem. Soc.* **1996**, *143*, 2558–2564.

[16] Hu, R.; Cola, B. A.; Haram, N.; Barisci, J. N.; Lee, S.; Stoughton, S.; Wallace, G.; Too, C.; Thomas, M.; Gestos, A., et al. Harvesting waste thermal energy using a carbon-nanotube-based thermo-electrochemical cell. *Nano Lett.* **2010**, *10*, 838–846.

[17] Nightingale, E. R. Phenomenological theory of ion solvation. Effective radii of hydrated ions. *J. Phys. Chem.* **1959**, *63*, 1381–1387.

[18] Burrows, B. Discharge behavior of redox thermogalvanic cells. *J. Electrochem. Soc.* **1976**, *123*, 154–159.

[19] Morais, E. A. D.; Alvial, G.; Longuinhos, R.; Figueiredo, J. M. A.; Lacerda, R. G.; Ferlauto, A. S.; Ladeira, L. O. Enhanced electrochemical activity using vertically aligned carbon nanotube electrodes grown on carbon fiber. *Mater. Res.* **2011**, *14*, 403–407.

[20] Kim, J. I.; Park, S. J. A study of ion charge transfer on electrochemical behaviors of poly(vinylidene fluoride)-derived carbon electrodes. *J. Anal. Appl. Pyrol.* **2012**, *98*, 22–28.

[21] Juan, Y.; Ke, Q. Preparation of activated carbon by chemical activation under vacuum. *Environ. Sci. Technol.* **2009**, *43*, 3385–3390.

[22] Babel, K.; Jurewicz, K. KOH activated carbon fabrics as supercapacitor material. *J. Phys. Chem. Solids* **2004**, *65*, 275–280.

[23] Bao, L.; Li, X. Towards textile energy storage from cotton T-shirts. *Adv. Mater.* **2012**, *24*, 3246–3252.

[24] Lota, G.; Fic, K.; Frackowiak, E. Carbon nanotubes and their composites in electrochemical applications. *Energ. Environ. Sci.* **2011**, *4*, 1592–1605.

[25] Kang, T. J.; Choi, A.; Kim, D. H.; Jin, K.; Seo, D. K.; Jeong, D. H.; Hong, S. H.; Park, Y. W.; Kim, Y. H. Electromechanical properties of CNT-coated cotton yarn for electronic textile applications. *Smart Mater. Struct.* **2011**, *20*, 015004.

[26] Cheng, Q.; Tang, J.; Ma, J.; Zhang, H.; Shinya, N.; Qin, L. C. Graphene and carbon nanotube composite electrodes for supercapacitors with ultra-high energy density. *Phys. Chem. Chem. Phys.* **2011**, *13*, 17615–17624.

[27] Hu, L.; Pasta, M.; Mantia, F. L.; Cui, L.; Jeong, S.; Deshazer, H. D.; Choi, J. W.; Han, S. M.; Cui, Y. Stretchable, porous, and conductive energy textiles. *Nano Lett.* **2010**, *10*, 708–714.

[28] Nugent, J. M.; Santhanam, K. S. V.; Rubio, A.; Ajayan, P. M. Fast electron transfer kinetics on multiwalled carbon nanotube microbundle electrodes. *Nano Lett.* **2001**, *1*, 87–91.

[29] Saliba, R.; Agricole, B.; Mingotaud, C.; Ravaine, S. Voltammetric and impedance analysis of dimethyldioctadecylammonium/Prussian blue Langmuir–Blodgett films on ITO electrodes. *J. Phys. Chem. B* **1999**, *103*, 9712–9716.

[30] Xiao, Y.; Lin, J. Y.; Tai, S. Y.; Chou, S. W.; Yue, G.; Wu, J. Pulse electropolymerization of high performance PEDOT/MWCNT counter electrodes for Pt-free dye-sensitized solar cells. *J. Mater. Chem.* **2012**, *22*, 19919–19925.

[31] Kang, T. J.; Fang, S. L.; Kozlov, M. E.; Haines, C. S.; Li, N.; Kim, Y. H.; Chen, Y. S.; Baughman, R. H. Electrical power from nanotube and graphene electrochemical thermal energy harvesters. *Adv. Funct. Mater.* **2012**, *22*, 477–489.

[32] Curtiss, C. F.; Bird, R. B. Multicomponent diffusion. *Ind. Eng. Chem. Res.* **1999**, *38*, 2515–2522.

[33] Eastman, E. D. Theory of the soret effect. *J. Am. Chem. Soc.* **1928**, *50*, 283–291.

[34] Eastman, E. D. Thermodynamics of non-isothermal systems. *J. Am. Chem. Soc.* **1926**, *48*, 1482–1493.

[35] deBethune, A. J.; Licht, T. S.; Swendeman, N. The temperature coefficients of electrode potentials: The isothermal and thermal coefficients—the standard ionic entropy of electrochemical transport of the hydrogen ion. *J. Electrochem. Soc.* **1959**, *106*, 616–625.

[36] Lu, X.; Xiao, Y.; Lei, Z.; Chen, J. Graphitized macroporous carbon microarray with hierarchical mesopores as host for the fabrication of electrochemical biosensor. *Biosens. Bioelectron.* **2009**, *25*, 244–247.

[37] Zhao, J.; Cheng, F.; Yi, C.; Liang, J.; Tao, Z.; Chen, J. Facile synthesis of hierarchically porous carbons and their application as a catalyst support for methanol oxidation. *J. Mater. Chem.* **2009**, *19*, 4108–4116.

[38] Wang, Z.; Kiesel, E. R.; Stein, A. Silica-free syntheses of hierarchically ordered macroporous polymer and carbon monoliths with controllable mesoporosity. *J. Mater. Chem.* **2008**, *18*, 2194–2200.

[39] Deng, Y.; Liu, C.; Yu, T.; Liu, F.; Zhang, F.; Wan, Y.; Zhang, L.; Wang, C.; Tu, B.; Webley, P. A., et al. Facile synthesis of hierarchically porous carbons from dual colloidal crystal/bock copolymer template approach. *Chem. Mater.* **2007**, *19*, 3271–3277.

[40] Li, Y.; Fu, Z. Y.; Su, B. L. Hierarchically structured porous materials for energy conversion and storage. *Adv. Funct. Mater.* **2012**, *22*, 4634–4667.

[41] Romano, M. S.; Li, N.; Antiohos, D.; Razal, J. M.; Nattestad, A.; Beirne, S.; Fang, S.; Chen, Y.; Jalili, R.; Wallace, G. G., et al. Carbon nanotube–reduced graphene oxide composites for thermal energy harvesting applications. *Adv. Mater.* **2013**, *25*, 6602–6606.